Bulletin of Faculty of Science, Zagazig University (BFSZU)
e-ISSN: 1110-1555
Volume-2023, Issue-2, pp-91-112
https://bfszu.journals.ekb.eg/journal
Research Paper DOI: **10.21608/bfszu.2023.177130.1210**

==========

Petrophysical and Rock Physics Analysis Using Well Log Data for Gas Detection in Scarab Gas Field, West Delta Deep Marine Concession, Egypt

Ashraf Ghoneimi[1], Muhammad Nabih[1], Mohamed Abd Elaziz [2,3], and Ahmed Bakry[1*]

[1] Zagazig University, Faculty of Science, Geology Department, 44519, Zagazig, Egypt
[2] Faculty of Computer Science and Engineering, Galala University, Suez 435611, Egypt
[3] Department of Mathematics, Faculty of Science, Zagazig University, Zagazig 44519, Egypt
Corresponding author: ambakry@science.zu.edu.eg

ABSTRACT **: The present study aims to detect the lithology and pore-fluid from well log data using the rock physics templates. The results show that we can potentially discriminate between different types of lithological facies and fluid type to predict the accumulations of the potential hydrocarbons. The cross-plotting technique of the rock properties is carried out using well log data from the Scrb field in the Western Offshore Nile Delta area. The available well log data; comprising the gamma-ray, resistivity, density, neutron and sonic logs were used. The interpretation of the log data shows a high resistivity, low GR, and low values of acoustic impedance, the gas-bearing interval is identified. To identify the rock attributes from the supplied log data, the petrophysical parameters are initially assessed before the conducting rock physics cross-plotting. This is achieved using the cross-plot of the Vp against Vs, density and Vp, Lambda-Rho and Mu-Rho, P-impedance and Poisson's ratio, P-impedance and Vp/Vs ratio, and Poisson's ratio and bulk modulus. The effective porosity (PHIE), shale volume (Vsh), water saturation (Sw), and hydrocarbon saturation (Sh) are used to color-code each cross plot. Cross-plotting is executed and Lambda Rho (λρ) cross-plots demonstrated to be more reliable for lithology determination than Vp against Vs cross-plots. The effective porosity average values are within the range from 24% to 30%, shale content within the range from 20% to 27%, water saturation within the range from 16% to 23%, hydrocarbon saturation ranges from 77% to 83%.**

KEYWORDS: **Scarab Gas Field; West Delta Deep Marine (WDDM); Acoustic impedance**

Date of Submission: 26-11-2022 Date of acceptance: 02-01-2023

I. INTRODUCTION

The Scarab gas field is located in the West Delta Deep Marine (WDDM) concession, at the mouth of the Nile, 63 kilometers to the northeast of the Rosetta branch **(Figure 1)**. The main hydrocarbon-bearing formation is the Late Pliocene El-Wastani Formation. The main reservoirs in this field are El-Wastani Formation Channels 1 and 2 (Ch-1 and Ch-2) (El-Gawad et al., 2019; Ghoneimi et al., 2021). Suites of logs comprise up the data collection that was made available for the present study, including GR, resistivity, DT (DTCO and DTSM), RHOZ and APLC logs in four wells of Scrb (Dd, Da, Db and 1, as illustrated in **Figure 1**).

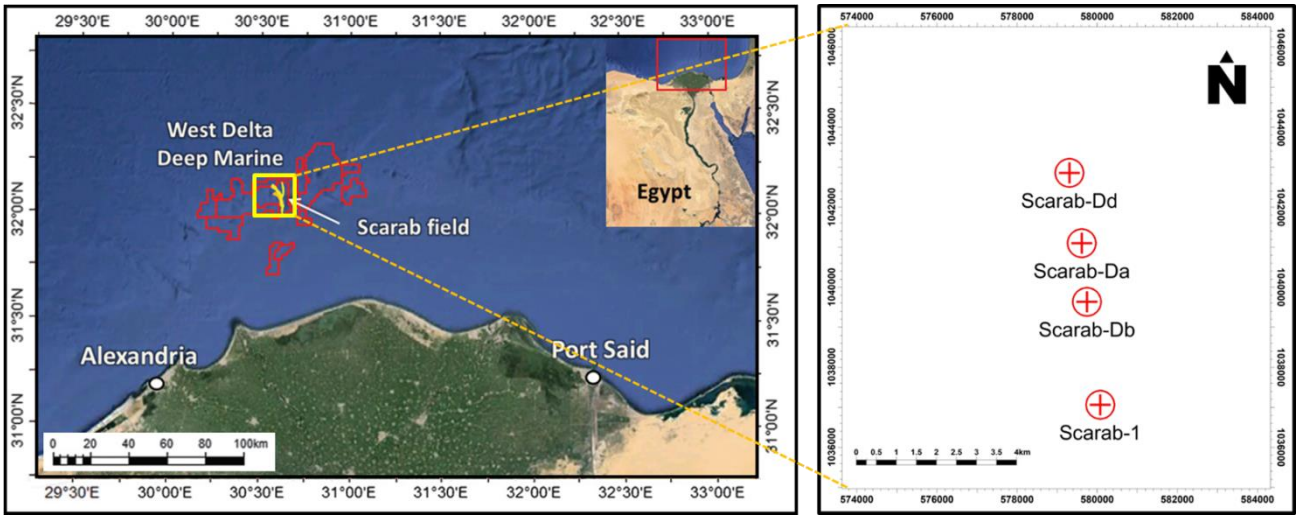

Figure 1: Location map of the WDDM concession, including Scarab Field (left) and base map of the available wells (right).

Estimation of the reservoir properties, such as lithology and pore fluid can be clearly determined by utilizing core samples. Nevertheless, the analysis for these purposes is costly and typically involves a huge amount of time and effort to get valuable information (Chang et al., 2002). Other geoscientists may establish outcomes from their analysis that are incompatible (Akinyokun et al., 2009). Similar to this, drilling cuttings can be used to identify reservoir characteristics. The biggest drawback of using such cuttings is that their recovery depth is frequently unknown, and most samples are typically too small to produce accurate and reliable results (Serra and Abbott, 1982). In order to get around these restrictions, there is rising interest in identifying reservoir features using well log data, which is relatively cheap and cost-effective. Additionally, well logging shows an interest in covering the entire geological formation of interest while also providing excellent basic information on the underground formation. In addition, Brigaud et al. (1990) noted that well logs provide a better picture of a lithological unit's in-situ conditions than do measurements made in a lab.

Due to the above-mentioned limitations of core analysis, rock physics is physics is a crucial method for an efficient geophysical interpretation, because of the vital connection between the lithology, geological deposition environment and pore fluid content of the reservoir rock (Nabih et al., 2022). The physical properties of a reservoir rock, such as its porosity, fluid incompressibility, and rock stiffness features, which affect how seismic waves pass through the rock, can be distinguished by the rock physics (Avseth, and Odegaard 2004; Avseth et al., 2005; Chi and Han, 2009).

Rock physics has recently developed into a vital instrument in petroleum geophysics and been essential in the quantitative interpretation of seismic data. Rock physics is used in the petroleum industry to improve reservoir forecasting and lower exploration-related hazards (Avseth et al., 2006). Additionally, elastic factors including velocity, density, acoustic impedance, and velocity ratio are used extensively in reservoir characterization studies, as well as their relationships to reservoir features. The porosity, shale content, water saturation, and hydrocarbon saturation are some of these reservoir characteristics. The same way, templates for describing an effective reservoir are made using rock physics modelling (Avseth and Odegaard, 2004; Andersen and Wijngaarden, 2007).

By looking at various points on the cross-plot of elastic characteristics, it is impossible to accurately forecast the lithology and saturation in the analysis of reservoir properties. Other petrophysical investigations depend on accurate recognition and comprehension of lithology, pore-fluid content, and pore shapes and sizes; these factors also make efficient tools for hydrocarbon exploration and production. Therefore, accurate information of these properties will be and remain the foremost challenge for the exploration and development of hydrocarbon reservoirs (Kupecz et al., 1997; Hami-Eddine et al., 2015). The determination of these properties helps in the detection of porosity, saturation, and permeability, and also helps petroleum and production engineers to take appropriate decisions

II. GEOLOGICAL SETTING

The WDDM concession, which is 50 to 100 km offshore of Egypt, covers the 6150 km2 northwestern edge of the Nile cone. The main structures are the NE-SW Rosetta fault trend and the offshore ENE-WNW Nile delta anticline trend (Mokhtar et al., 2016). The geological column of the Nile Delta represents the Late Eocene-Oligocene period **(Figure 2**). (2014) Sharaf et al. Recent exploration efforts have been concentrated on the Pliocene-Pleistocene strata, which contain the main gas reservoirs.

The geology of the WDDM concession and the Scarab field is composed of a complicated system of undersea channels made up of sands with varied reservoir qualities that are dispersed in irregularly shaped, occasionally interconnected tiny traps. The background geology of dirty sand and shale is characterised by substantial lateral variation. Sheet sands and splays, which could be gas bearing and challenging to resolve with traditional seismic techniques, could be expected as thin beds.

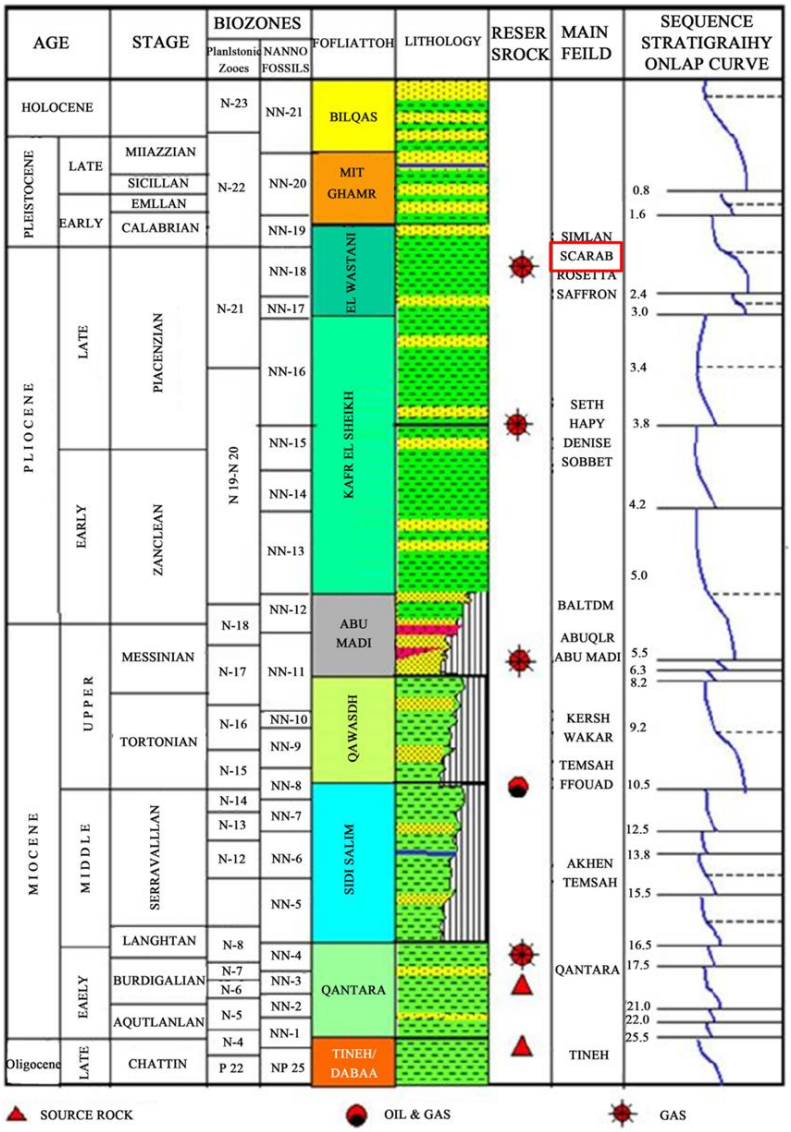

Figure 2: Generalized litho-stratigraphic column of the WDDM concession, containing Scarab field (Rio et al. 1991; Raslan, 2002).

III. METHODOLOGY

Petrophysics and rock physics are conducted for the four available wells in the current study. Each well also provides compressional and shear wave velocity logs in addition to gamma, resistivity, density, and neutron logs (**Figures 4 to 7**). These logs are used to calculate elastic parameters, rock physics characteristics, and petrophysical properties. The petrophysical characteristics that are

estimated include Vsh, PHIE, Sw, Sh, and net-pay thickness. The AI, Vp/Vs ratio, Poisson's ratio, K, and Mu-Rho are all calculated and used for the study of rock physics.

Petrophysical Analysis

The well log analysis main target is to evaluate the formation to estimate the Vsh, PHIE, Sw, Sh and net-pay thickness. The log analysis software Interactive Petrophysics (v4.4) is used to perform this complex iterative operation for formation evaluation.

Shale content (Vsh) aids to distinguish between relatively low-shale reservoir and relatively high-shale non reservoir. Because that radioactivity of shale is higher than that of sand rocks, gamma-ray logs are utilized to determine the content of shale. (Abd Elaziz et al., 2022). The basic equations expressing the relation between the intensity of natural gamma-ray radiation and volume of shale (Dresser Atlas, 1979) are:

$$I_{GR} = \frac{GR_{log} - GR_{min}}{GR_{max} - GR_{min}}$$

which can is corrected to Vsh using the equation of Larionov (1969):

$$Vsh = 0.083\ (23.7\ IGR - 1)$$

where:

IGR: gamma ray index,
GRlog: gamma ray reading at interest interval,
GRmin: minimum gamma ray (clean sand),
GRmax: maximum gamma ray (shale).

The effective porosity is a crucial parameter for assessment of reservoir properties. In this work, from density-neutron combination the effective porosity is calculated utilizing the following equations (Asquith et al., 2004 and Bateman, 2012):

$$\emptyset_{NC} = \emptyset_N - (V_{sh} * \emptyset_{Nsh})$$
$$\emptyset_{DC} = \emptyset_D - (V_{sh} * \emptyset_{Dsh})$$
$$\emptyset_e = \sqrt{\frac{(\emptyset_{DC})^2 + (\emptyset_{NC})^2}{2}}$$

where:

$\emptyset_{NC}$ = Corrected neutron porosity,
$\emptyset_N$ = Neutron porosity,
$\emptyset_{Nsh}$ = Apparent neutron porosity in shale,
V_{sh} = Shale volume,
$\emptyset_{DC}$ = Corrected density porosity,
$\emptyset_D$ = Density porosity,
$\emptyset_{Dsh}$ = Apparent density porosity in shale,
$\emptyset_e$ = Effective porosity.

To determine fluid saturation, one must first distinguish between the various fluid components (water or hydrocarbons). The Indonesian equation is utilized to calculate water saturation (Schlumberger, 1972):

$$S_w^n = \frac{1}{R_t} / [\sqrt{\frac{\emptyset_e{}^m}{a.R_w}} + \frac{V_{sh}{}^{(1-0.5V_{sh})}}{\sqrt{R_{sh}}}]^2$$

where:

R_t = True formation resistivity,
V_{sh} = Shale volume,
R_w = Formation water resistivity,
R_{sh} = Shale resistivity
S_w = Water saturation,
$\emptyset_e$ = Effective porosity,
a = Tortuosity constant,
m = Cementation factor
n = Saturation exponent

Then, the hydrocarbon saturation is estimated from: $S_h = 1 - S_w$

The net pay is calculated by applying suitable cutoffs for output petrophysical properties for that the unproductive layers are not estimated. Cutoffs are mainly applied to PHIE, Vsh, and Sw. The used cutoffs are Vshmax 35%, Phiemin 10% and Swmax 50%, the results are shown in **Figures 4, 5, 6 and 7**.

Rock physics analysis

Several rock physics models and templates are largely necessary for the workflow in the field of rock physics. Any model of rock physics shows the connections between the physical traits of various rocks (Simm and Bacon, 2014). Rock physics modelling, which makes use of the interdependency between these features and generates the possibility of generating a more exact and unambiguous image, improves the output of a model (Maulana, 2016).

By identifying the elastic characteristics and pore fluids of the rocks, the rock physics template (RPT) bridges the connections between seismic data and geology and helps to illustrate reflection signatures. Models aid in comprehension of non-reservoir zones and reservoir behaviour. Avseth and Odegaard (2004) provided examples of rock physics templates, and the majority of them are used to analyse or categorise seismic inversion data for the potential presence of hydrocarbons during exploration.

The RPT which demonstrates the relations between the acoustic impedance (AI) and Vp/Vs ratio **(Figure 3)** displays the idea of the most popular rock physics relations. The template includes sand fluid saturation patterns and porosity trends for several lithologies (Rasaq et al, 2015). Arrows are frequently used to illustrate other geological trends, including deposition, burial compaction, and pressure.

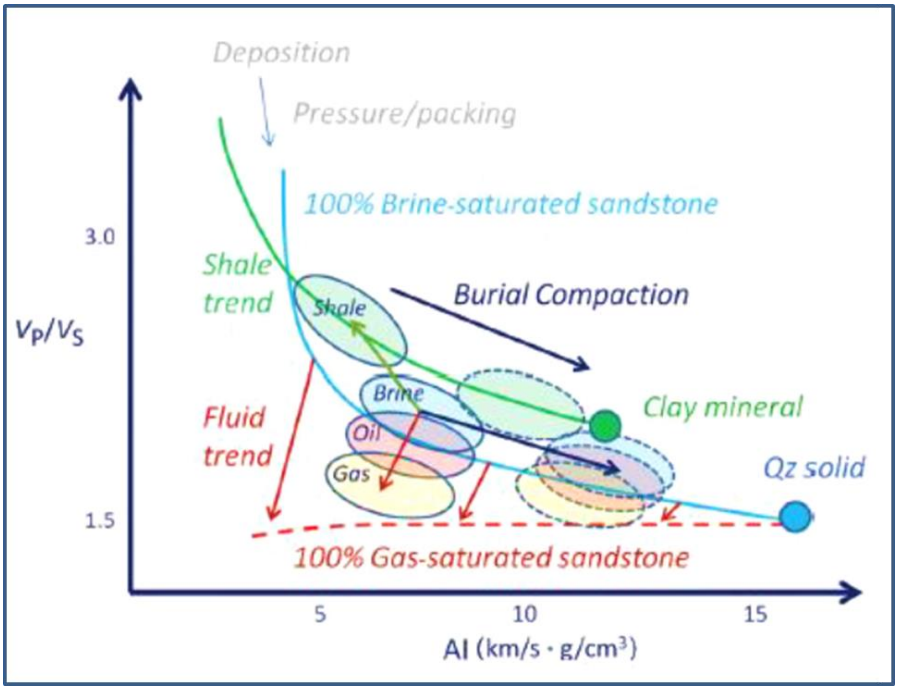

Figure 3: RPT idea for shale and gas- and brine-saturated sandstone (Avseth and Veggeland, 2015).

In the present study, the following equations are used to calculate the rock physics parameters:

$$K = \rho\,(V_P{}^2 - \frac{4}{3}V_S{}^2)$$

$$\sigma = \frac{V_P{}^2 - 2V_S{}^2}{2(V_P{}^2 - V_S{}^2)}$$

$$\mu = \rho\, V_S{}^2$$

$$\frac{V_P}{V_S} = \sqrt{\frac{1-\sigma}{0.5-\sigma}}$$

Where:

K = Bulk modulus

σ = Poisson's ratio

μ = Shear modulus

ρ = Density
V_P = Compressional velocity wave
V_S = Shear velocity wave

By checking the relations of additional rock physics, it has been found that the Lame's rock parameters (i.e. incompressibility*density and rigidity*density) (Goodway et al., 1997) provided superior discrimination of Scarab lithologies.

The incompressibility and rigidity of the rocks and pore fluids are characterized by the properties that result from merging the impedances of Vp and Vs, which rely on the density and the Lame's parameter (Austin et al., 2018). Plotting of these attributes will be more useful for differentiating fluids and lithologies, assuming that shales are less rigid than sandstones, water-filled sandstones are more rigid than gas-filled sandstones, and that shales are less compressible than sandstones. The fluid incompressibility ($\lambda\rho$) is estimated utilizing the equation:

$$\lambda\rho = I_P{}^2 - 2I_s{}^2$$

where I_P is P-wave acoustic impedance (ρVp) in m/s*g/cc and I_s is S-wave acoustic impedance (ρVs) in m/s*g/cc. The rock rigidity ($\mu\rho$) is estimated utilizing the relation:

$$\mu\rho = 2I_s{}^2$$

where $\mu\rho$ is the rock rigidity in Gpa*g/cc and I_s is S-wave acoustic impedance in m/s*g/cc. The Mu-Rho is a very sensitive property to the rock rigidity "stiffness" which reflects the rock forming minerals. Sandstone, composed mainly of quartz is more rigid than the clay minerals forming shale. Accordingly, the Mu-Rho of the sandstone reservoirs is more than that of the shale.

IV. RESULTS AND DISCUSSION

The GR, resistivity, RHOZ, APLC, Vp, and Vp/Vs, Ip logs, in addition to lithology, are the available input data utilized in the present study. The logs and the gas zones that were identified in the wells of Scrb-1, Scrb-Db, Scrb-Da, and Scrb-Dd are shown in **Figures 4, 5, 6, and 7**, respectively. These well logs are used to estimate output results as Vsh, PHIE, Sw, and pay net flag.

Sands, which have lower GR values, can be distinguished from the shale zone, which have lower GR values, on the GR curve. Ch-2 is obviously more shale than ch-1, especially in Scrb-Da well.

The assessment of fluid saturations and thickness of the hydrocarbons are the main uses of the resistivity logs. There may be hydrocarbons present because ch 1 and 2 in the Scrb-Dd well, as well as ch 1 in the Scrb-1, Scrb-Da, and Scrb-Db wells, all have high resistivity values.

The most used tools for estimating porosity and lithology, as well as for gas detection, are density and neutron log combinations. The crossover that is visible in the wells of Scrb-1, Scrb-Da, Scrb-Db, and Scrb-Dd is an indication of gas intervals.

To estimate porosity and the mechanical characteristics of rocks, the Vp log is employed. Additionally, it is frequently used to identify rocks that contain gas because the P-wave velocity typically drops off dramatically in gas-bearing zones. The type of saturated fluid has an impact on the compressive wave velocity. In ch 1 and 2 of the Scrb-Dd well, as well as ch 1 of the wells of Scrb-1, Scrb-Da, and Scrb-Db, the P-wave velocity slightly reduces.

Utilizing the velocity ratio (Vp/Vs) is crucial for determining the amount of pore fluid present, the degree of consolidation, and lithology. The presence of gas causes the Vp/Vs ratio value in reservoir zones to slightly decrease.

Acoustic impedance is the result of the P-wave velocity and bulk density (AI). Evaluation of the pore fluid and lithology is the acoustic impedance log's main application. In interesting gas reservoirs, the value of the AI is slightly reduced.

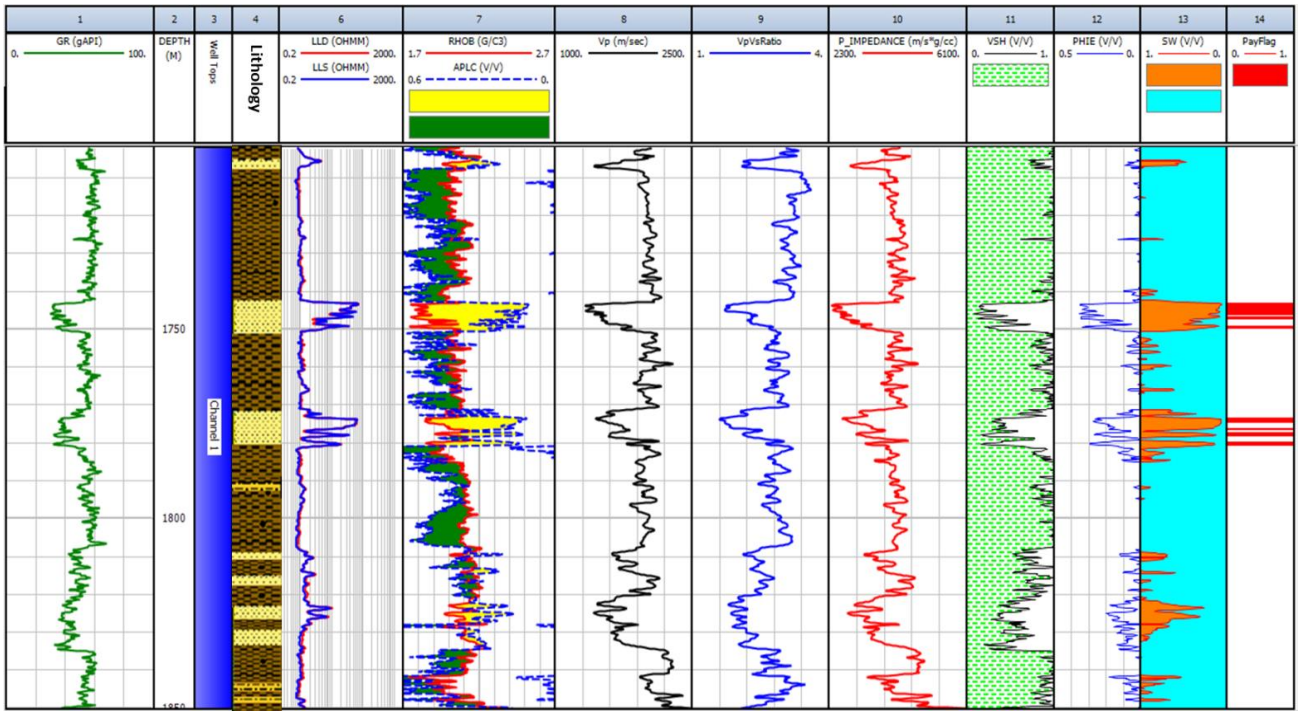

Figure 4: Scrb-1 well input data (GR, lithology, resistivity, density-neutron, Vp, Vp/Vs., Ip) and output (VSH, PHIE, SW, SH and net pay).

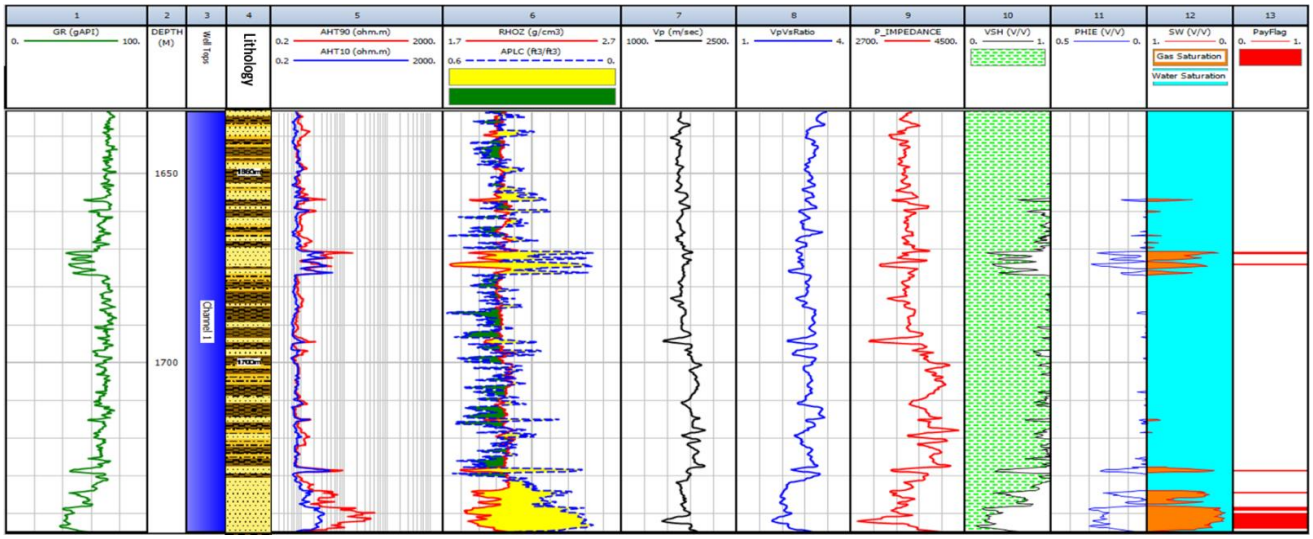

Figure 5: Scrb-Db well input data (GR, lithology, resistivity, density-neutron, Vp, Vp/Vs., Ip) and output (VSH, PHIE, SW, SH and net pay)

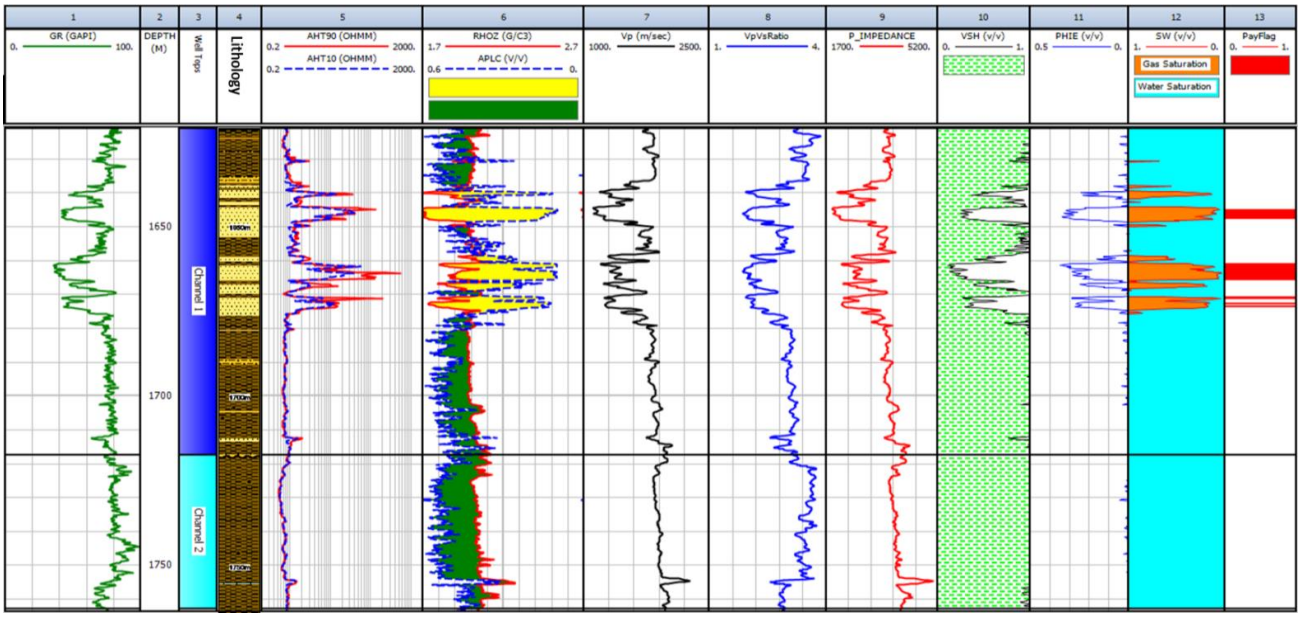

Figure 6: Scrb-Da well input data (GR, lithology, resistivity, density-neutron, Vp, Vp/Vs., Ip) and output (VSH, PHIE, SW, SH and net pay).

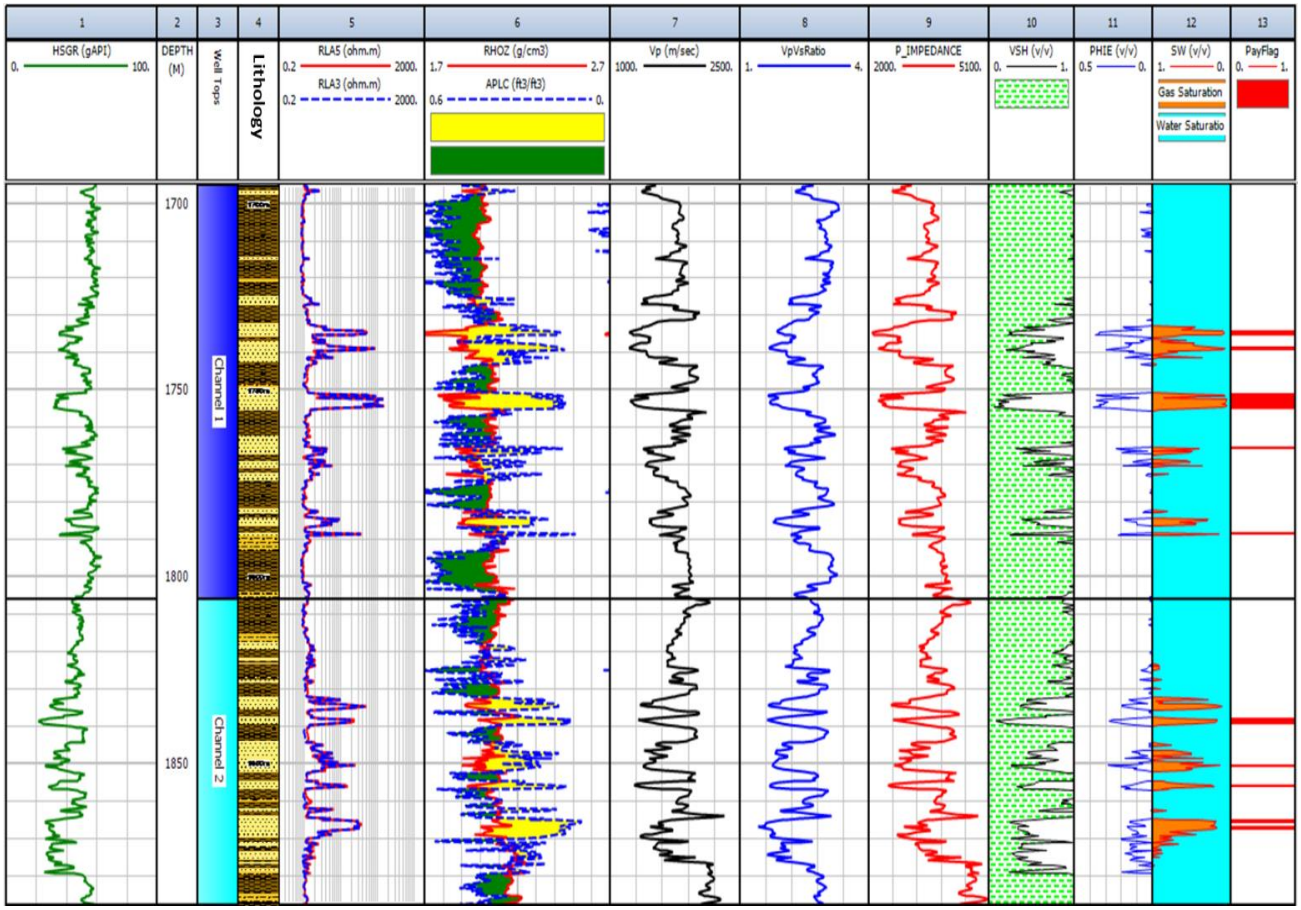

Figure 7: Scrb-Dd well input data (GR, lithology, resistivity, density-neutron, Vp, Vp/Vs., Ip) and output (VSH, PHIE, SW, SH and net pay).

The average petrophysical parameter values obtained for ch-1 in the four wells are demonstrated by histograms in **Figure 8**. The maps of the distribution of these petrophysical

properties are shown in **Figure 9**. The inspection of the histograms and maps demonstrate some degree of matching between most of the petrophysical properties.

The histograms and maps show that the sand thickness, and consequently the net pay, are remarkably higher in wells Scrb-1 and Da, while in wells Scrb-Db and Dd have relatively lower values. The histogram demonstrates that while water saturation is proportionally related to and rises with shale content, effective porosity and hydrocarbon saturation have an inverse connection with it. The hydrocarbon saturation is proportionally associated with and increases with the effective porosity. The other petrophysical parameters have no relationship to the net pay thickness.

The iso-parametric maps (**Figure 9**) show that the effective porosity, hydrocarbon saturation and net pay, increase toward the north direction while shale volume and water saturation increase toward the south. The effective porosity average values are within the range from 24% to 30%, shale content within the range from 20% to 27%, water saturation within the range from 16% to 23%, hydrocarbon saturation ranges from 77% to 83%, and the net pay thickness is within 5 to 8 m.

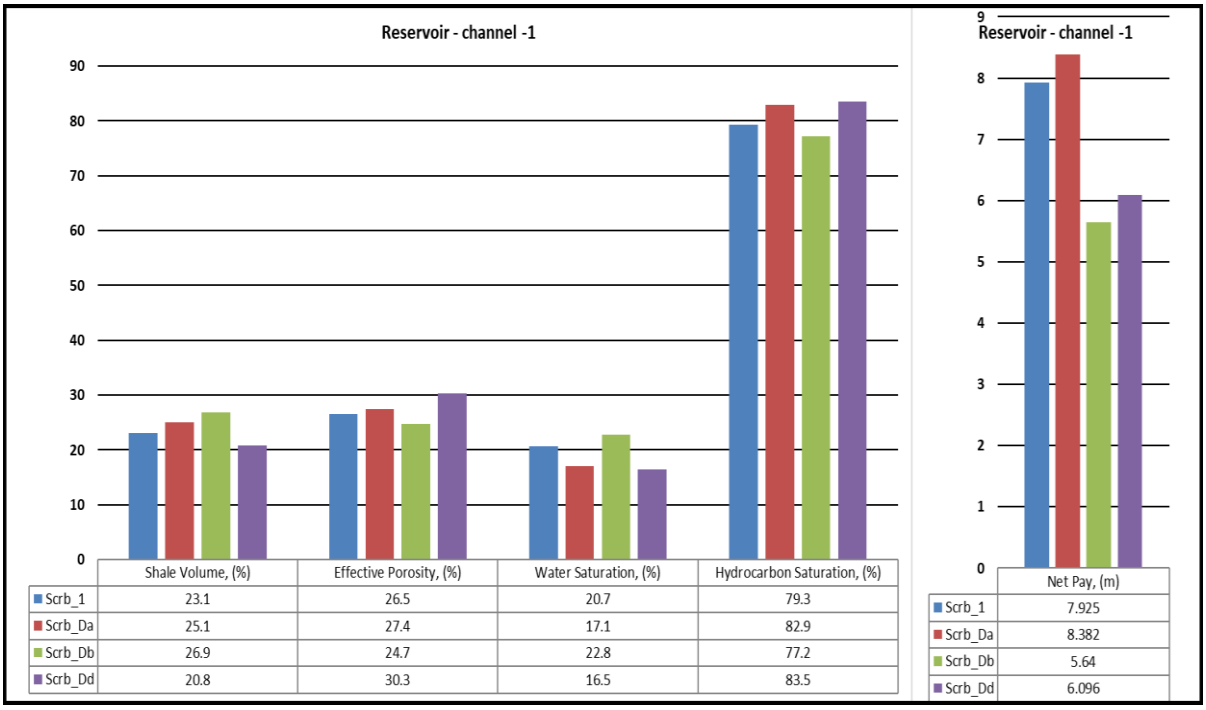

	Shale Volume, (%)	Effective Porosity, (%)	Water Saturation, (%)	Hydrocarbon Saturation, (%)
Scrb_1	23.1	26.5	20.7	79.3
Scrb_Da	25.1	27.4	17.1	82.9
Scrb_Db	26.9	24.7	22.8	77.2
Scrb_Dd	20.8	30.3	16.5	83.5

	Net Pay, (m)
Scrb_1	7.925
Scrb_Da	8.382
Scrb_Db	5.64
Scrb_Dd	6.096

Figure 8: Petrophysical parameters histogram of Ch-1in four wells

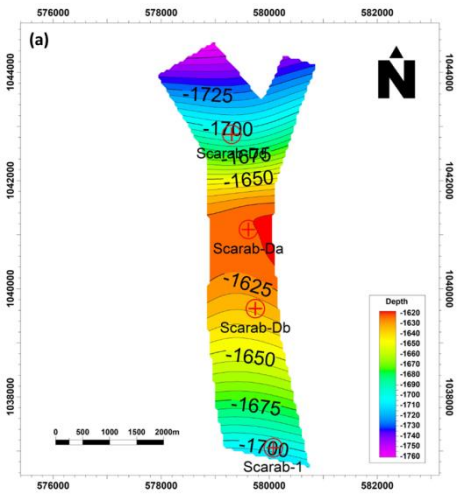

Depth map for top of channel 1

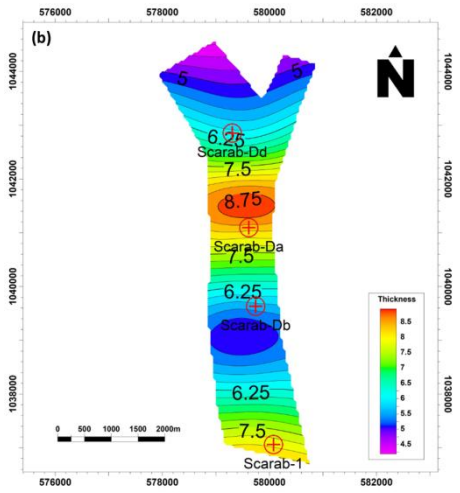

Reservoir thickness map

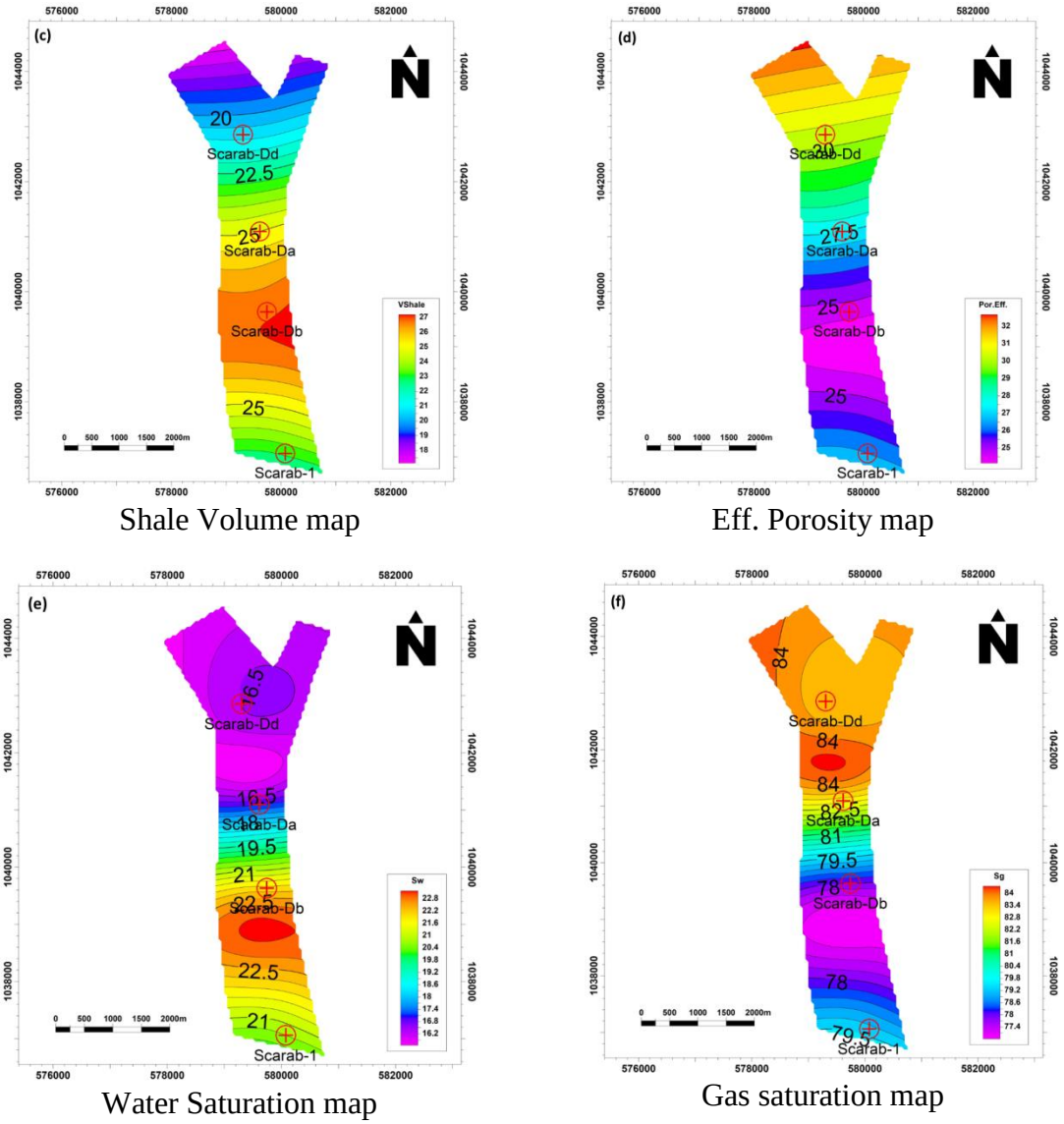

Shale Volume map | Eff. Porosity map

Water Saturation map | Gas saturation map

Figure 9: Petrophysical parameters distribution maps of Ch-1

The RPT of ch-1 is applied using the Scrb-Db well. (**Figures 10 to 15**). The parameters of the studied rock physics are cross-plotted with each other, such as Vp-Vs, ρb (RHOZ)-Vp, Ip-Poisson's ratio, λρ-μρ, Poisson's ratio-K and Ip-Vp/Vs ratio (**Figures 10 to 15**) for ch-1. The Vsh, PHIE, Sw, and Sh are used to color-code these cross-plots. These templates are plotted to demonstrate their accuracy in separating the cross-plotted points based on lithology and fluid content, as well as in differentiating between intervals of shale and gas sand.

The cross-plot of Vp versus Vs (**Figure 10**) shows that basing on the shale color-coding (**Figure 10-a**), Vp discriminates between shale and gas-sand points while Vs does not clearly distinguish between them where both shale and gas-sand points have low Vs values. According to the PHIE, Sw, and Sh color coding (**Figure 10-b, c and d**), the same as above is shown but with more differentiation with Vp and less differentiation for Vs. In the four plots, the shale points have greater Vp values than gas-sand points, and the gas-sand points have somewhat higher Vs values.

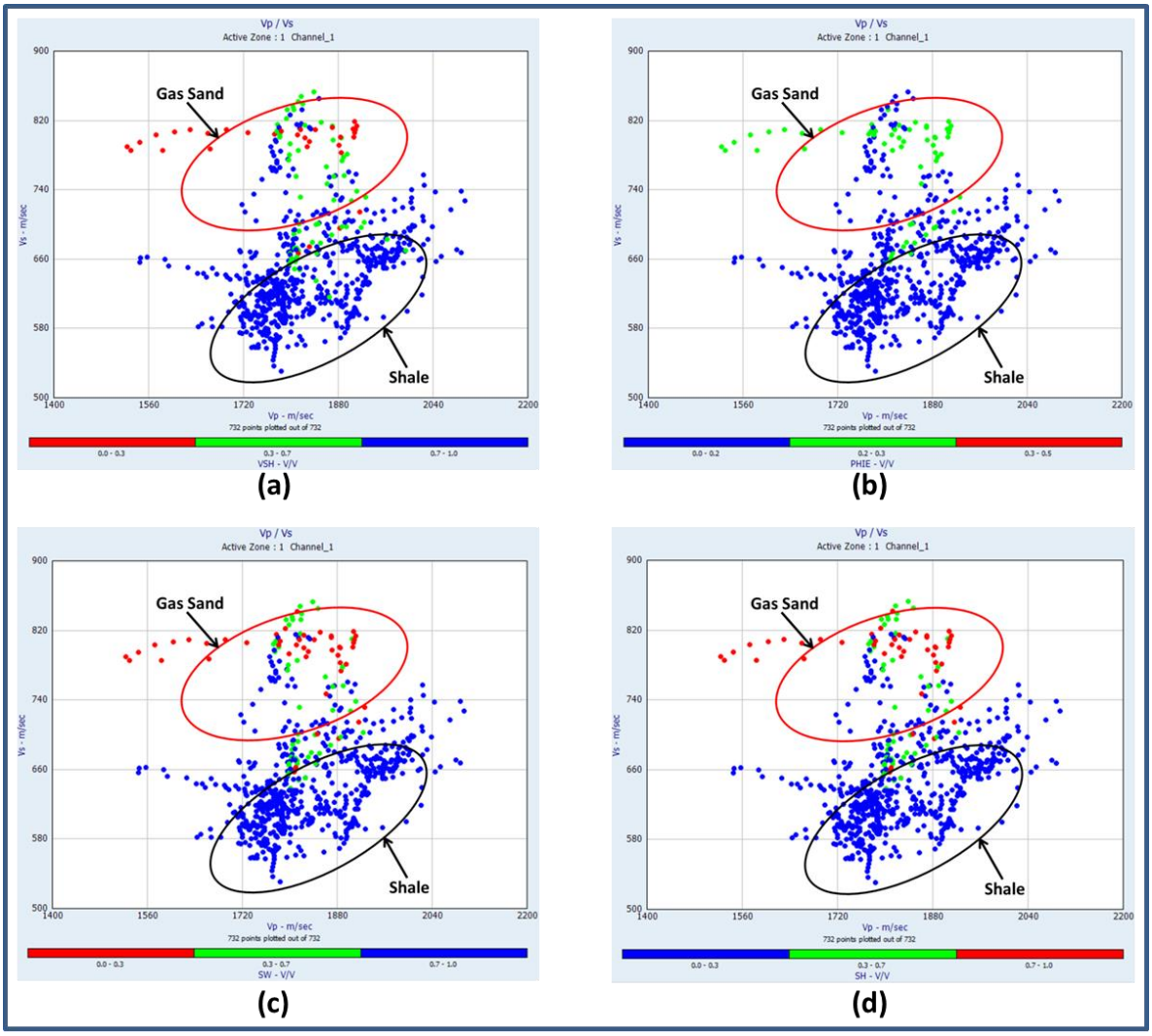

Figure 10: Crossplots of Vp against Vs of Scrb-Db well, according to color coding of VSH, PHIE, SW, and SH, respectively.

In the cross-plot of ρb (RHOZ) against Vp (**Figure 11),** and basing on the color coding of either Vsh, PHIE, Sw or Sh, the discrimination between the shale and gas-sand points is more than that above. The shale points have higher density and P-wave velocity than the gas-sand points.

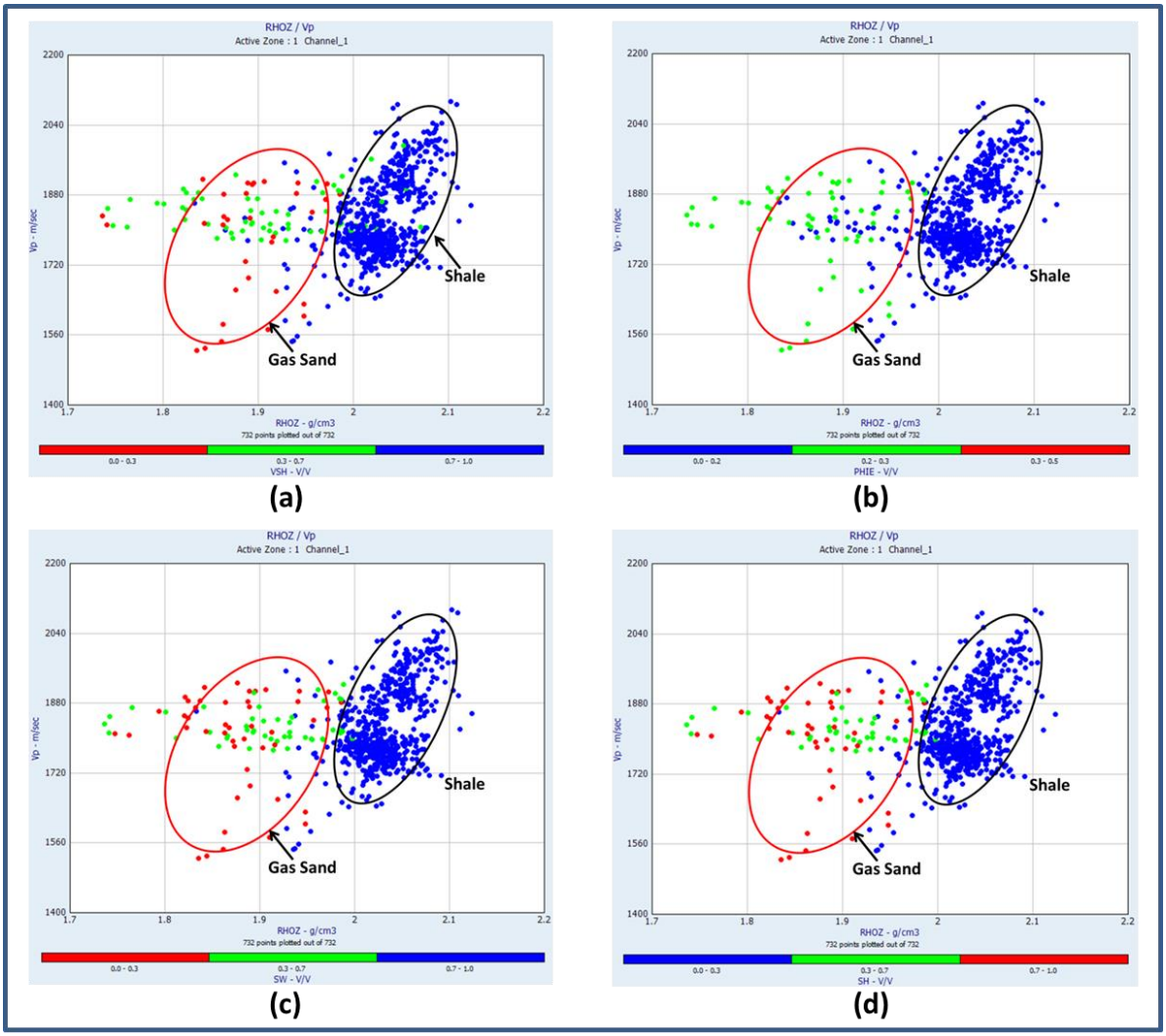

Figure 11: Crossplots of RHOZ versus Vp of Scrb-Db well, according to color coding of VSH, PHIE, SW, and SH, respectively.

The cross-plot of P-impedance versus Poisson's ratio and based on the Vsh, Sw and Sh color-coding **(Figure 12-a, c and d)**, Poisson's ratio distinguishes between shale and gas-sand points more clearly than the P-impedance, which has less discriminating between the two types of points. The differentiation according to the PHIE color coding **(Figure 12-b)** is more than the previous ones.
Figure 13 shows the cross-plot between Lambda-Rho against Mu-Rho. According to the color-coding of Vsh, Sw and Sh, Shale and gas-sand points are distinguished easily by Lambda-Rho (**Figure 13-a, c, and d**), whereas Mu-Rho is less obvious. According to the PHIE color coding (**Figure 13-b**), there is less differentiation using Lambda-Rho. Shale has more Lambda-Rho points than gas sand does in all plots. Compared to gas-sand points, shale points have a somewhat lower Mu-Rho value.

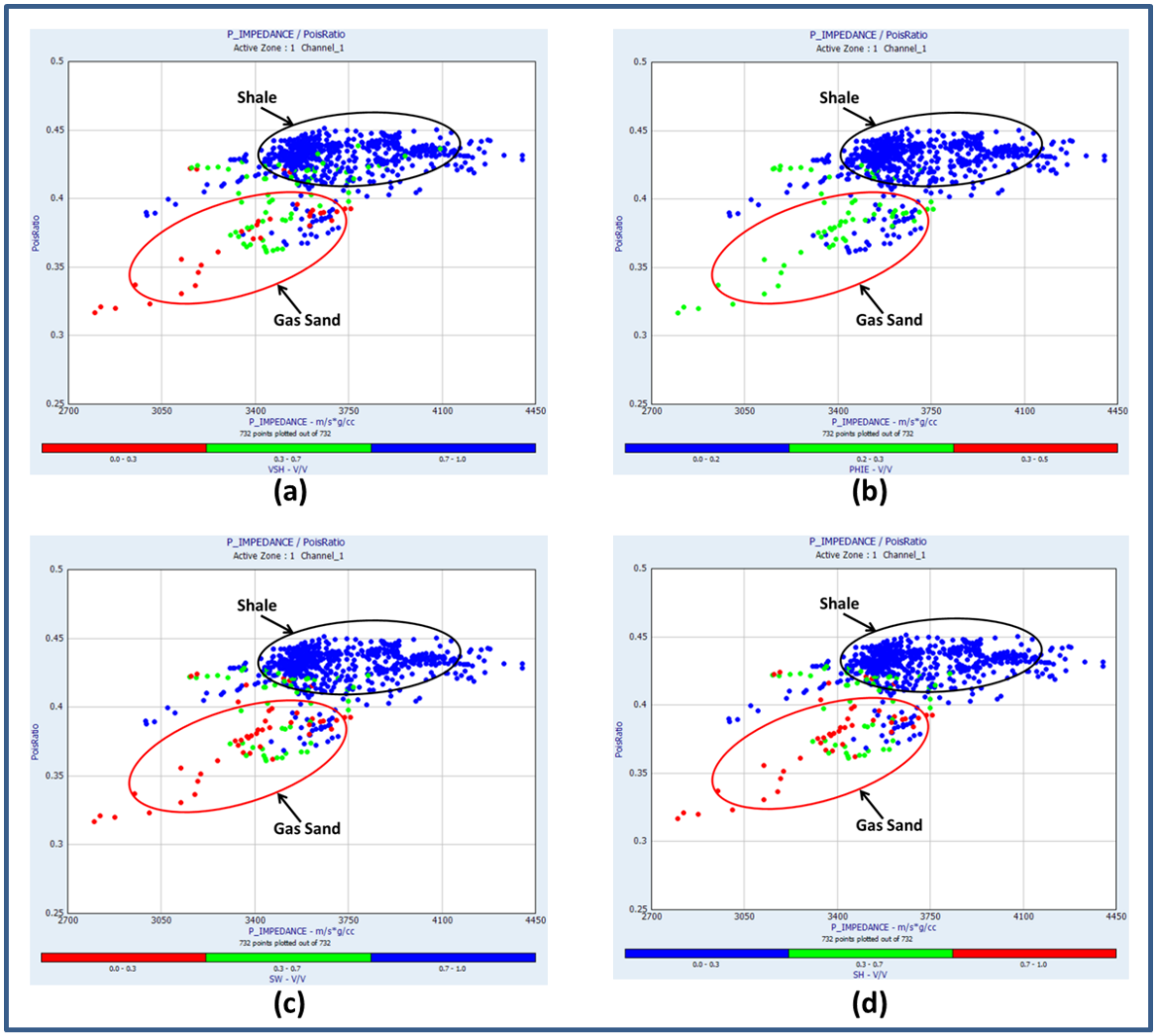

Figure 12: Crossplots of Ip against Poisson's ratio of Scrb-Db well, according to color coding of VSH, PHIE, SW, and SH, respectively.

The cross-plots shown in **Figure 14** is made between the Poisson's ratio and bulk modulus and colored by Vsh, PHIE, Sw and Sh, respectively. In these plots, the gas-bearing sand is distinguished clearly from shale points, where the gas-sand has lower values of both Poisson's ratio and bulk modulus compared to the shale. **Figure 14-a** shows some overlap between the gas-sand and shale points more than that based on other parameters (PHIE, Sw and Sh).

Figure 15 shows the P-impedance and Vp/Vs ratio plots and and using color code according to Vsh, PHIE, Sw and Sh, respectively. According to the Vsh color coding, Shale and gas-sand points can be distinguished using Ip and velocity ratio. According to PHIE, Sw, and Sh color coding less distinction occurs between gas-sand and shale points. AI and Vp/Vs ratio rise when shale content does as well.

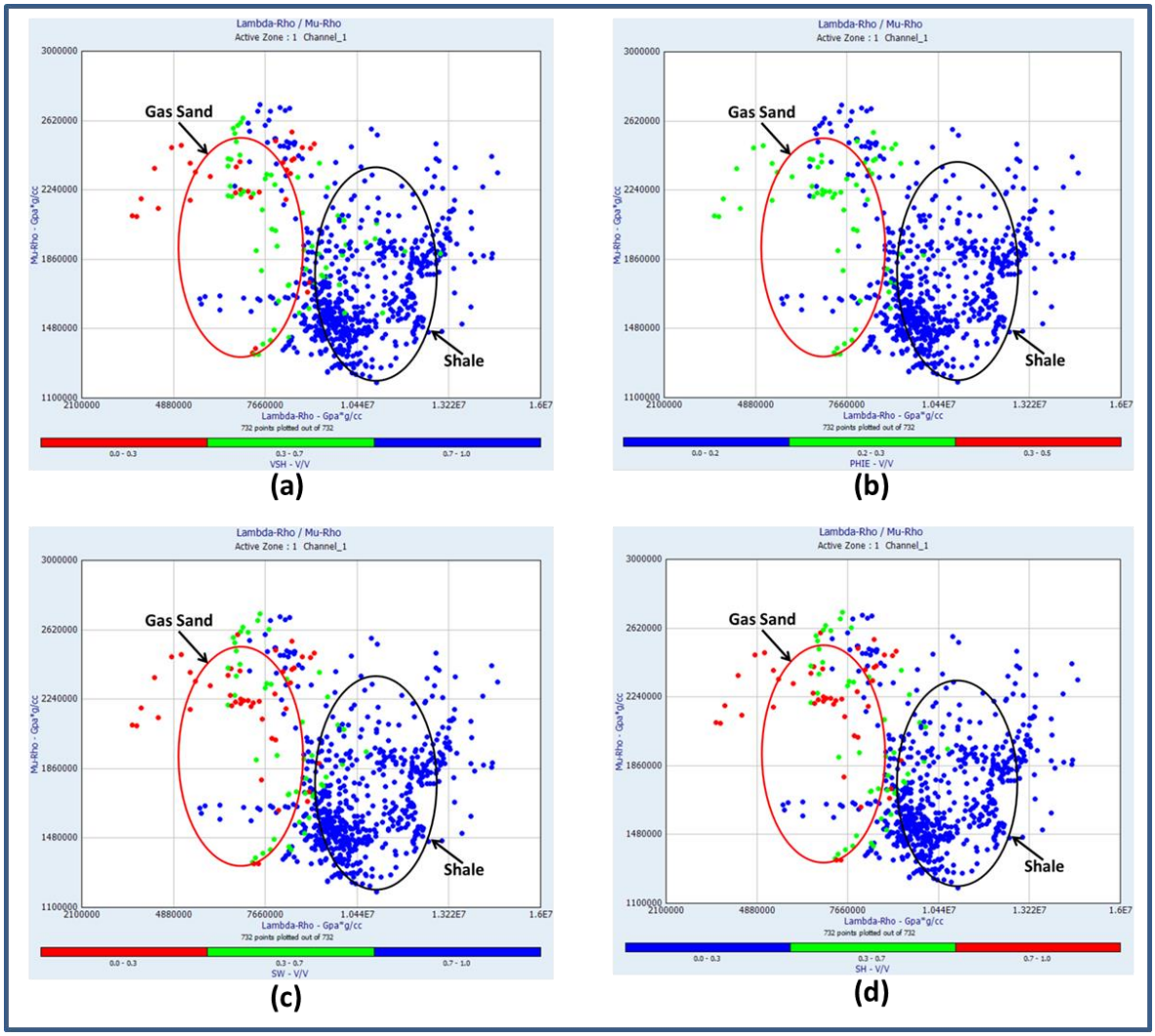

Figure 13: Plots of Lambda-Rho against Mu-Rho of Db well, Scrb-Db well, according to color coding of VSH, PHIE, SW, and SH, respectively.

In addition to the above relations, the plots of the bulk density, P-wave velocity and P-impedance versus depth are plotted for ch-1 in the Scrb-Db well (**Figures 16, 17 and 18**) and colored based on Vsh, PHIE, Sw and Sh, respectively. Generally, it is clearly revealed in **Figure 16** that the density increases with depth as shown by the main trend of the points, this may be due to the increase of compaction with depth. The local fluctuations of the density-depth relation are due to lithology and fluid-content. The intervals of anomalous minimum density are due to the presence of gas bearing sand. The increase of water saturation and shale content increases the bulk density.

Figure 17 shows the p-wave velocity increases with depth as shown by the main trend of the points. This may be due to the increase of bulk density and compaction with depth. The local oscillations of the P-wave velocity with depth are due to lithology and fluid-content. The intervals of abnormal minimum p-wave velocity are due to the presence of gas-bearing sand. The presence of water-saturated and shale zones increases the P-wave velocity.

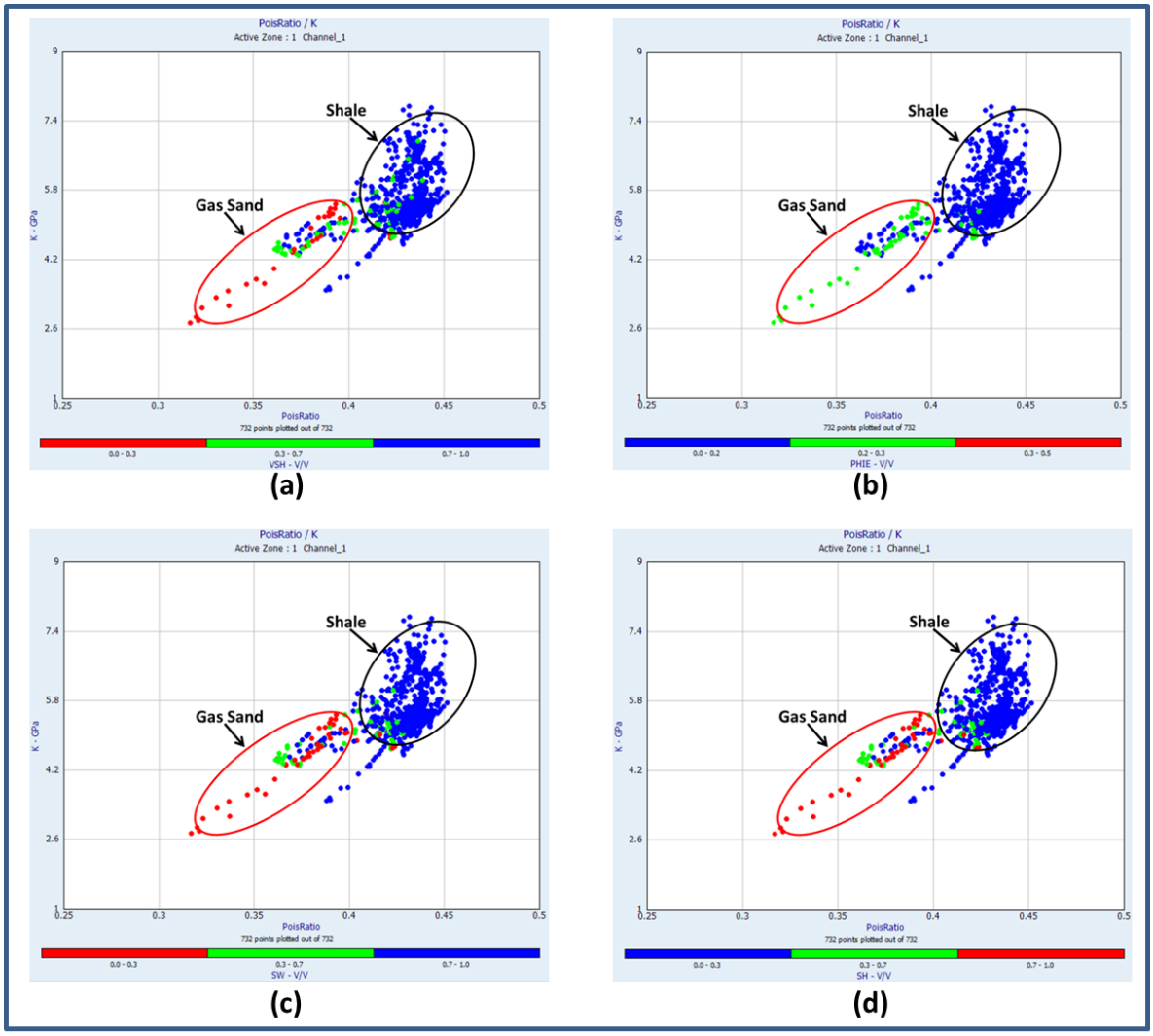

Figure 14: Crossplots of Poisson's ratio versus bulk modulus of Scrb-Db well, according to color coding of VSH, PHIE, SW, and SH, respectively.

The plot of the P-impedance versus depth for Scrb-Db well **(Figure 18)** shows that there is a general trend of the points revealing that the P-impedance increases with depth. This may be due to the increase of compaction, density and P-wave velocity with depth. The local variations of the P-impedance with depth are due to lithology, porosity and fluid-content. The intervals of anomalous minimum P-impedance are due to the presence of gas-bearing sand. In contrast, the presence of water-saturated and shale intervals increases the P-impedance.

In the same manner, plotting the other rock physics parameters (Poisson's ratio, $\lambda\rho$, bulk modulus (K) and Vp/Vs ratio) versus depth will give similar patterns. This is due to their similar characteristics with Vsh, PHIE, Sw and Sh and their capability to distinguishe between gas-sand and shale intervals.

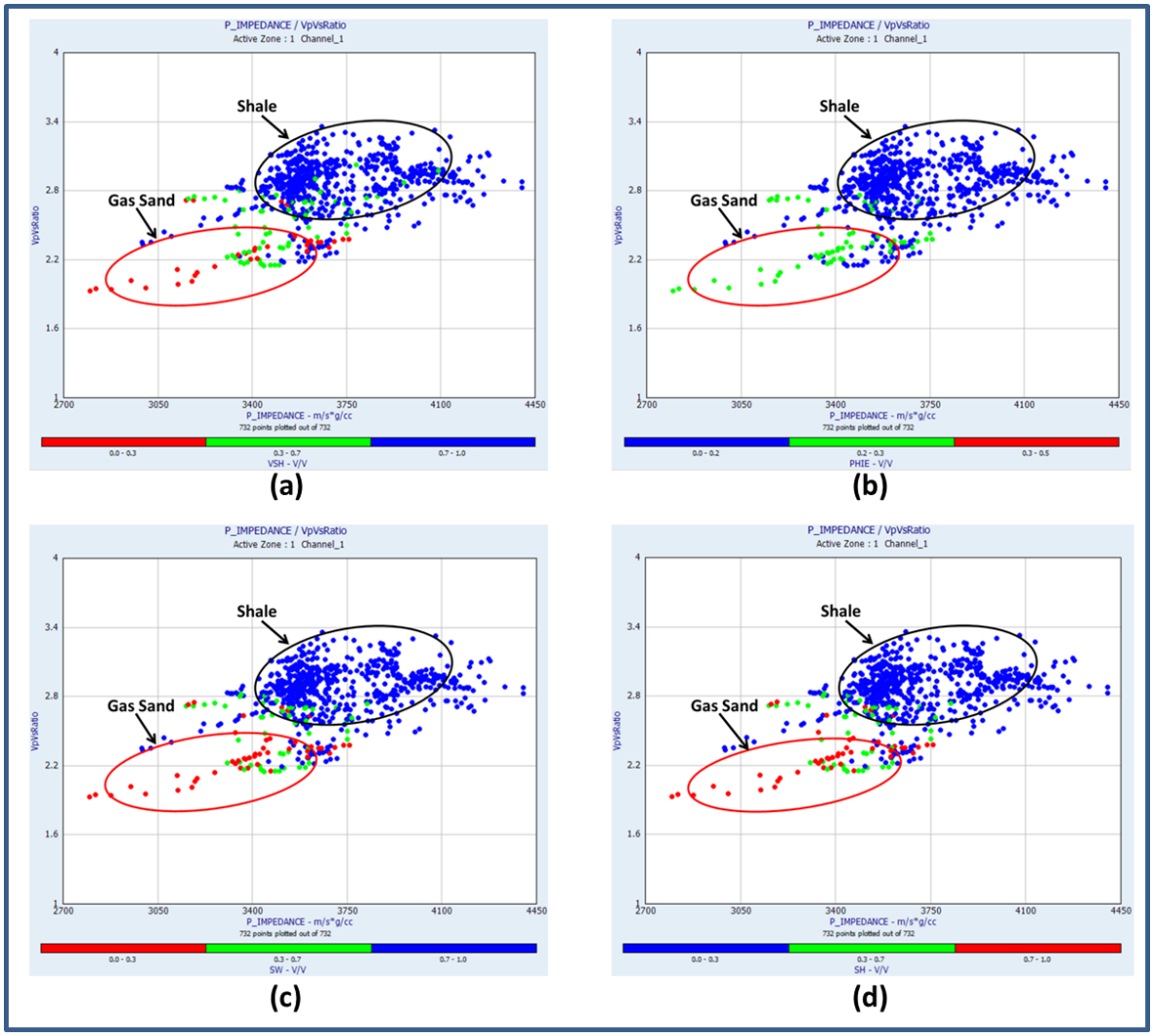

Figure 15: Plots of Ip against (Vp/Vs) of Db well, Scrb-Db well, according to color coding of VSH, PHIE, SW, and SH, respectively.

For ch-1 in the four wells, the estimated average values for the rock physics parameters are demonstrated by histograms in **Figure 19** and are mapped to show their distribution laterally along the channel path as shown in **Figure 20**. The inspection of these histograms and maps demonstrate some degree of matching and relations between some of the rock physics parameters.

The histograms and maps demonstrate that the bulk modulus and Lambda-Rho are significantly larger in wells Scrb-1 and Db, but the wave velocity (Vp) and P-impedance are noticeably higher. The histograms demonstrate a proportionate relationship between the bulk modulus, P-impedance, and Lambda-Rho and the wave velocity (Vp). Other aspects of rock physics are not clearly related. According to the iso-parametric contour maps (Figure 20), rock physics characteristics generally decrease in the direction of the north. Comparing these results with that of the petrophysical characteristics demonstrate that the decrease of the rock physical parameters is associated with the growth of the effective porosity and gas saturation towards the northern half of the study area.

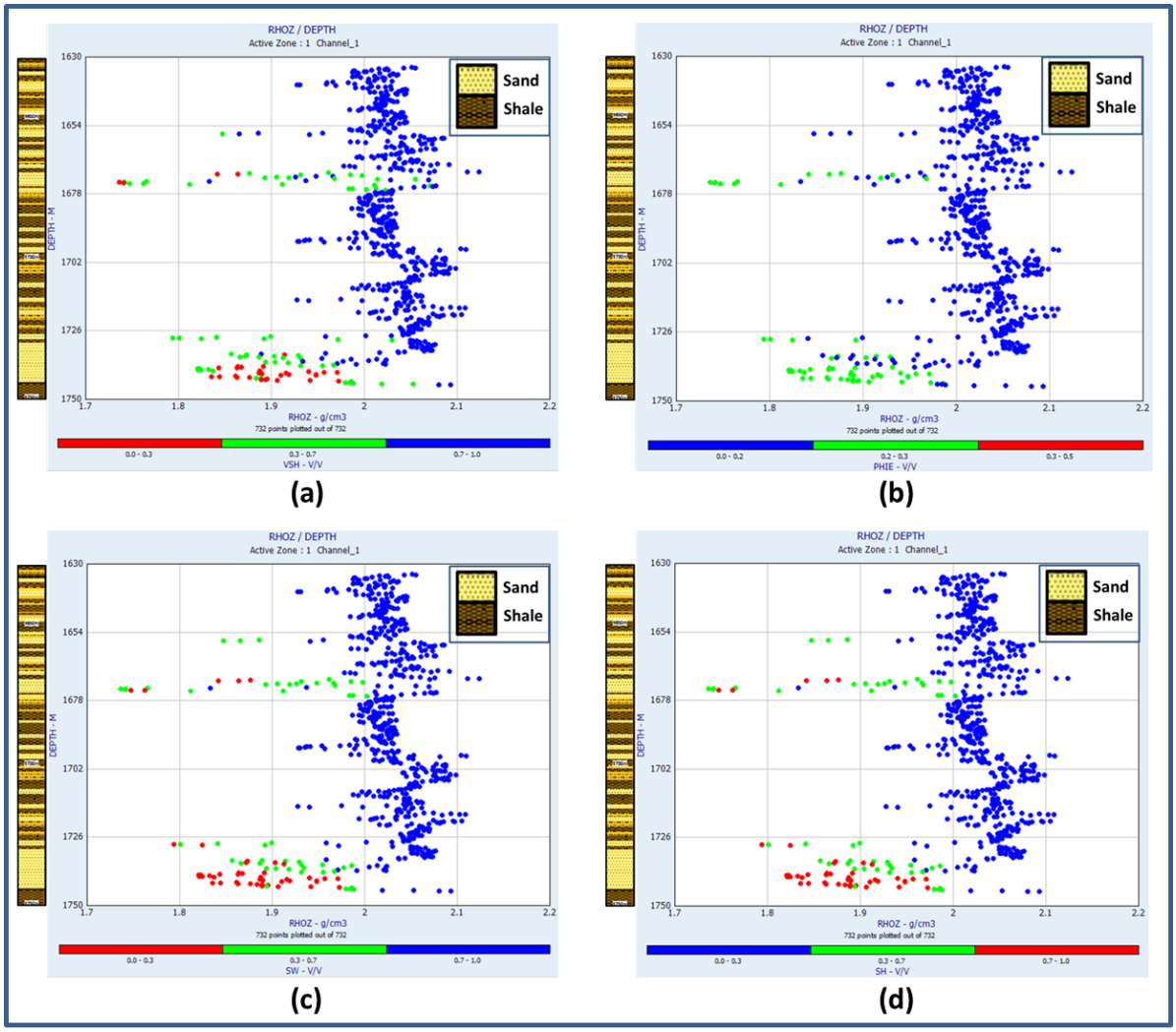

Figure 16: Crossplots of RHOZ versus depth of Db well, Scrb-Db well, according to color coding of VSH, PHIE, SW, and SH, respectively.

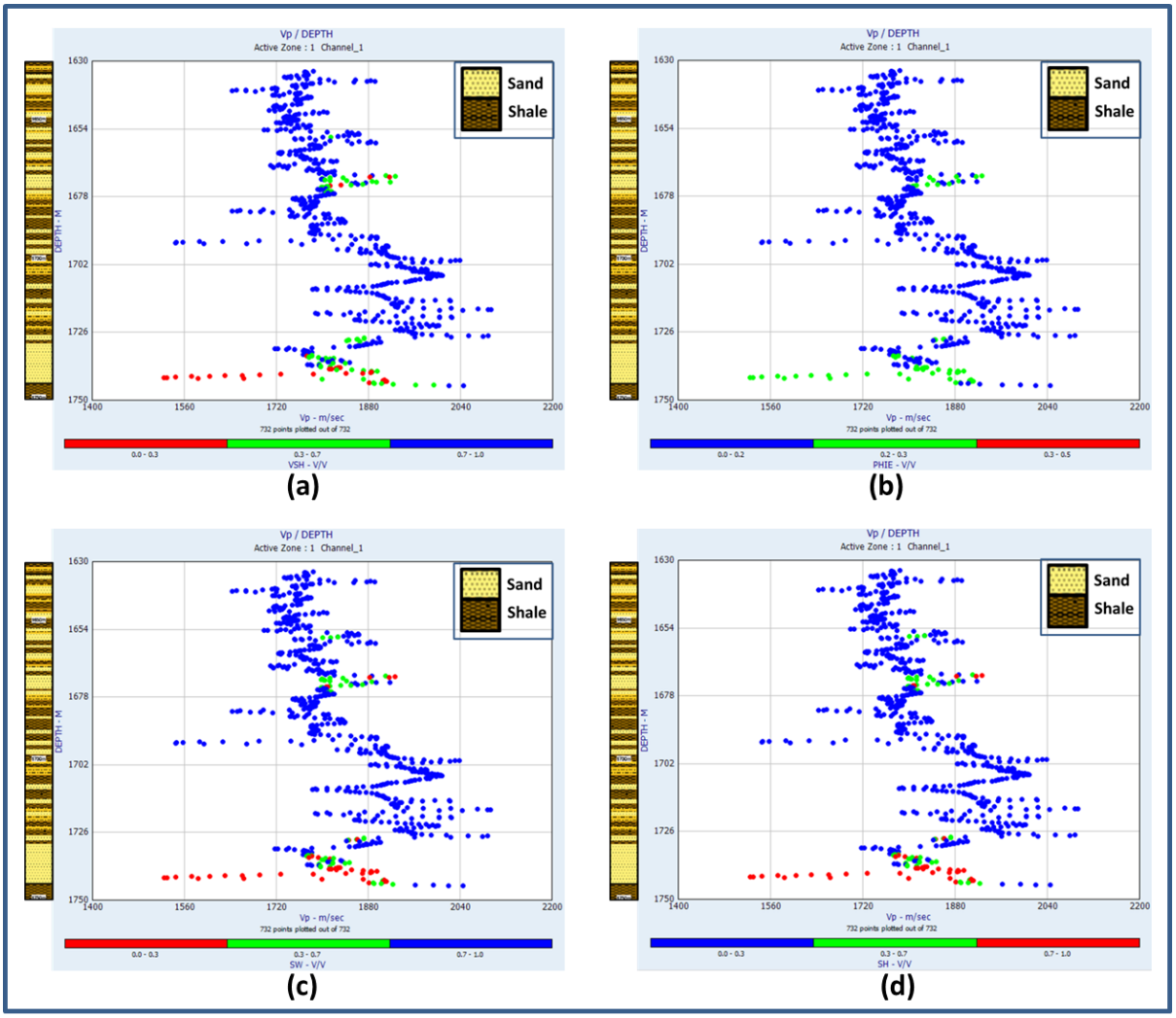

Figure 17: Crossplots of Vp versus depth of Db well, Scrb-Db well, according to color coding of VSH, PHIE, SW, and SH, respectively.

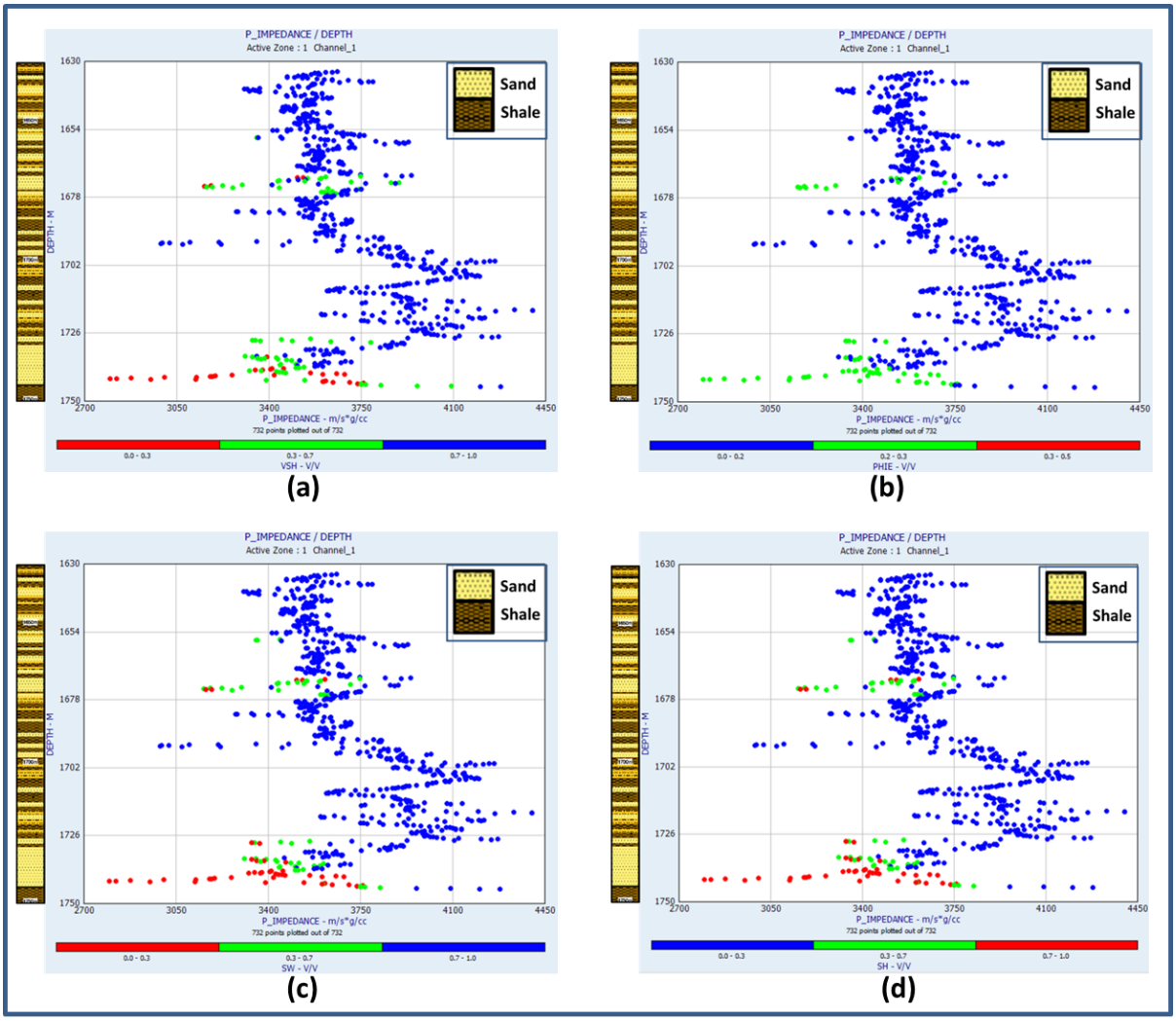

Figure 18: Crossplots of P-impedance versus depth of Db well, Scrb-Db well, according to color coding of VSH, PHIE, SW, and SH, respectively.

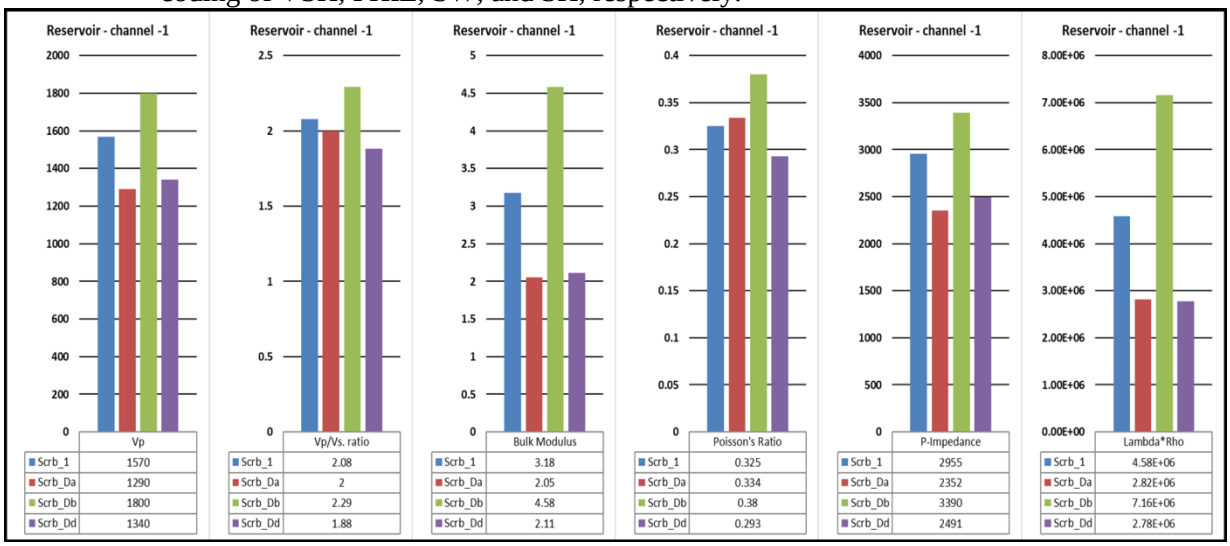

Figure 19: Histogram of the rock physics parameters of Ch-1 1in the four wells

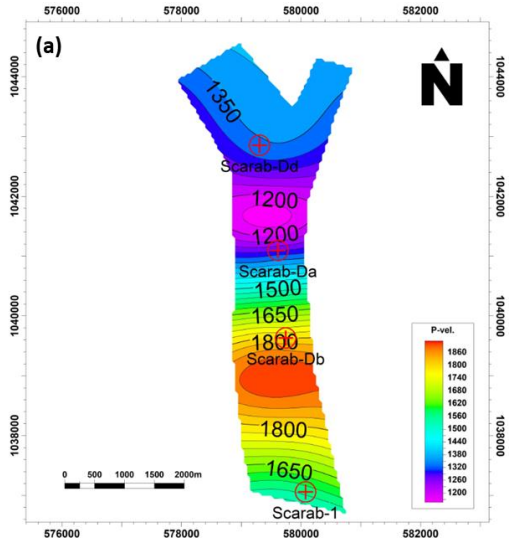

P-Wave Velocity map

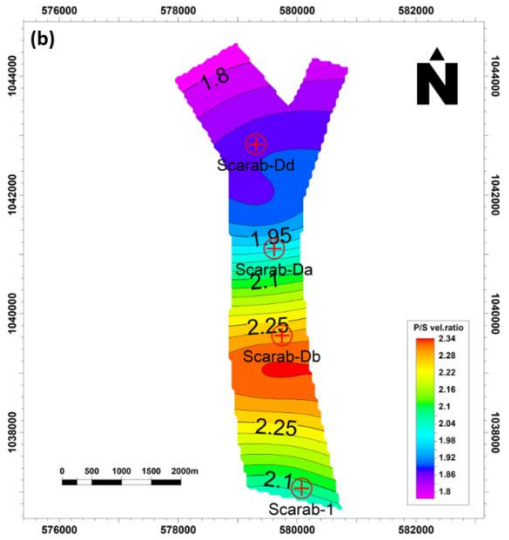

Vp/Vs. Ratio map

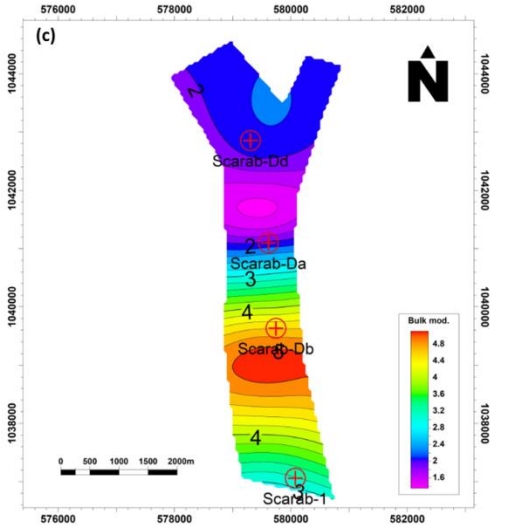

Bulk Modulus map

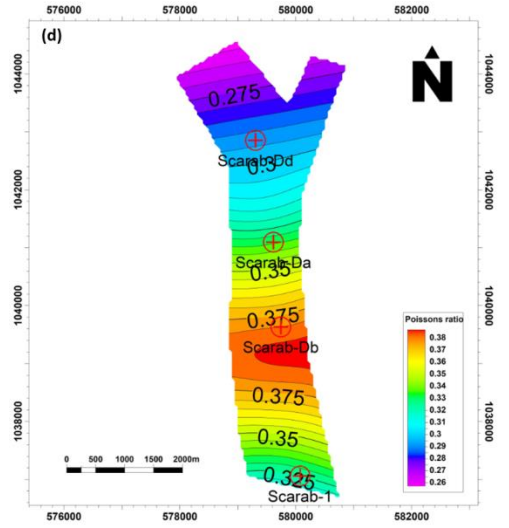

Poisson's ratio map

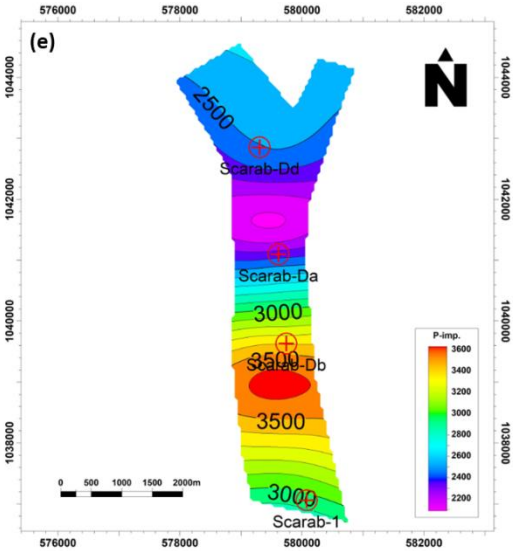

P-impedance map

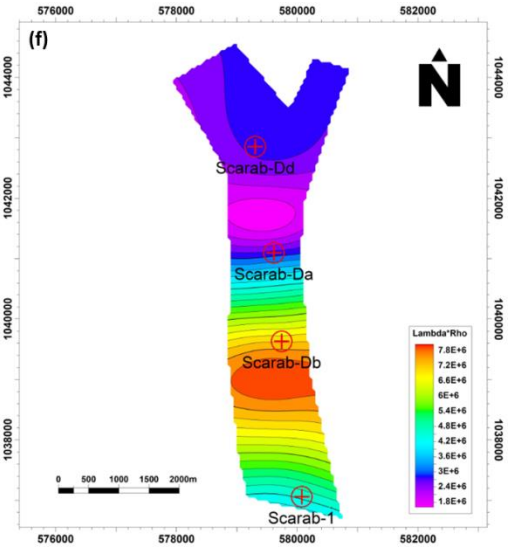

Lambda*Rho map

Figure 20: Rock physics parameters distribution maps of Channel-1

V. CONCLUSIONS

This study demonstrates how the well log data can be effectively used to distinguish the lithology and fluid saturation of reservoirs using the rock physics templates. Cross plots have been shown to be effective tools for illustrating how different combinations of log responses affect lithology and fluid prediction. The cross-plots of the Scrb-Db well are used to evaluate reservoir rock properties and understand how lithology and fluids influence reactions. The plots of density versus P-wave velocity, Ip and Poisson's ratio, Poisson's ratio against K, and Ip against Vp/Vs ratio are the best tools for identifying gas sand and shale intervals. These cross plots demonstrate lower values for density, P-wave velocity, Ip, Poisson's ratio, K, Lambda-Rho, and velocity ratio in the gas-sand intervals compared to the shale intervals. The iso-parametric maps of petrophysical characteristics reveal an increase in shale volume and water saturation toward the south of the research area and a rise in effective porosity, hydrocarbon saturation, and net pay toward the north. Rock physics parameter distribution maps reveal a general decline in the northern direction, which is equal to an increase in gas saturation in the same direction.

ACKNOWLEDGMENT

The authors appreciate both the EGPC and RASHPETCO Company for giving the well log data of the area of study.

REFERENCES

Abd Elaziz, M., Ghoneimi, A., Elsheikh, A. H., Abualigah, L., Bakry, A., Nabih, M., 2022. Predicting Shale Volume from Seismic Traces Using Modified Random Vector Functional Link Based on Transient Search Optimization Model: A Case Study from Netherlands North Sea. Natural Resources Research, 1-17.

Akinyokun, O.C., Enikanselu, P.A., Adeyemo, A.B., Adesida, A., 2009. Well log interpretation model for the determination of lithology and fluid contents. The Pacific Journal of Science and Technology, 10 (1), 507-517.

Andersen, C.F., Wijngaarden, A.V., 2007. Interpretation of 4D AVO inversion results using rock physics templates and virtual reality visualization. In: North Sea examples: 77th Annual International Meeting, SEG, Expanded Abstracts, 77, 2934–2938.

Asquith, G., Krygowski, D., Henderson, S., Hurley, N., 2004. Basic well log analysis (Second Edition). The American Association of Petroleum Geologists (AAPG), Tulsa, Oklahoma, 229. ISBN: 0-89181-667-4.

Austin, O.E., Agbasi, O.E., Samuel, O., Etuk, S.E., 2018. Cross plot analysis of rock properties from well log data for gas detection in Soku field, Coastal Swamp Depobelt, Niger Delta Basin. Journal of Geoscience, Engineering, Environment, and Technology, 3 (4), 180-186.

Avseth, P., Mukerji, T., Mavko, G., 2005. Quantitative seismic interpretation: Applying rock physics tools to reduce interpretation risk. Cambridge University Press.

Avseth, P., Veggeland, T., 2015. Seismic screening of rock stiffness and fluid softening using rock physics attributes. Interpretation, 3 (4), SAE85-SAE93.

Avseth, P., Wijngaarden, A.J., Mavko, G., Johansen, T.A., 2006. Combined porosity, saturation net-to-gross estimation from rock physics templates: 76th Annual Meeting, SEG, Expanded Abstracts, 1856–1860.

Avseth, P.A., Odegaard, E., 2004. Well log and seismic data analysis using rock physics templates. First break, 22 (10).

Bateman, R.M., 2012. Open hole log analysis and formation evaluation. Second Edition, Society of Petroleum Engineers (SPE), ISBN 978-1-61399-156-5, ISBN 978-1-61399-269-2 (Digital), 653p.

Brigaud, F., Chapman, D. S., Le Douaran, S., 1990. Estimating thermal conductivity in sedimentary basins using lithologic data and geophysical well logs. AAPG Bulletin, 74(9), 1459-1477.

Chang, H., Kopaska-Merkel, D., Chen, 2002. Identification of lithofacies using Kohonen self-organizing maps. Comput. Geosci. 28, 223–229.

Chi, X., Han, D., 2009. Lithology and fluid differentiation using rock physics templates. The Leading Edge, 28, 60–65.

Dresser Atlas, 1979. Log interpretation charts: Houston. Texas, Dresser Industries Inc, 107.

El-Gawad, A., El-Aziz, A., Abd El-Moktader, N., 2019. Reservoir quality determination through petrophysical analysis of El-Wastani Formation in Scarab field, offshore Nile Delta, Egypt. Al-Azhar Bulletin of Science, 30(1-D), 1-12.

Ghoneimi, A., Farag, A. E., Bakry, A., Nabih, M., 2021. A new deeper channel system predicted using seismic attributes in scarab gas field, west delta deep marine concession, Egypt. Journal of African Earth Sciences, 177, 104155.

Goodway, B., Chen, T., Downton, J., 1997. Improved AVO fluid detection and lithology discrimination using Lamé petrophysical parameters;"λρ","μρ", and "λ/μ fluid stack", from P and S inversions. In SEG Technical Program Expanded Abstracts 1997 (183-186). Society of Exploration Geophysicists.

Hami-Eddine, K., Klein, P., Loic, R., Ribet, B., Grout, M., 2015. A new technique for lithology and fluid content prediction from prestack data: An application to carbonate reservoir. pp. 1.

Kupecz, J.A., Gluyas, J., Bloch, S., 1997. Reservoir quality prediction in sandstones and carbonates. American Association of Petroleum Geologists, 69.
DOI: https://doi.org/10.1306/M69613.

Larionov, V.V., 1969. Radiometry of boreholes (in Russian). Nedra, Moscow.

Maulana, T., 2016. Quantitative seismic interpretation using rock physics templates-case examples from the Zumba field (Master's thesis, NTNU).

Mokhtar, M., Saad, M., Selim, S., 2016. Reservoir architecture of deep marine slope channel, Scarab field, offshore Nile Delta, Egypt: Application of reservoir characterization. Egyptian Journal of Petroleum, 25(4), 495-508. DOI.org/10.1016/j.ejpe.2015.11.003.

Nabih, M., Ghoneimi, A., Bakry, A., Chelloug, S. A., Al-Betar, M. A., Abd Elaziz, M., 2022. Rock physics analysis from predicted Poisson's ratio using RVFL based on Wild Geese Algorithm in scarab gas field in WDDM concession, Egypt. Marine and Petroleum Geology, 147, 105949.

Rasaq, B., Igwenagu, C.L., Onifade, Y.S., 2015. Cross plotting of rock properties for fluid and lithology discrimination using well data in a Niger delta oil field. Journal of Applied Sciences and Environmental Management, 19 (3), 539-546.

Raslan, S., 2002. Sedimentology and sequence stratigraphic studies for Scarab-Saffron field. Ph. D. Thesis, Faculty of Science, Ain Shams University, Cairo, Egypt.

Rio, D., Sprovieri, R., Thunell, R., 1991. Pliocene-lower Pleistocene chronostratigraphy: a re-evaluation of Mediterranean type sections. Geol. Soc. Am. Bull. 103, 1049-1058.

Schlumberger, 1972. The essential of log interpretation practice. Copyright, France. 14, 154-155.

Serra, O.T., Abbott, H.T., 1982. The contribution of logging data to sedimentology and stratigraphy. Society of Petroleum Engineers Journal, 22 (01), 117-131.

Sharaf, E., Korrat, I., Seisa, H., Esmaiel, E., 2014. Seismic imaging and reservoir architecture of sub-marine channel systems offshore west Nile Delta of Egypt. Open Journal of Geology, 4, 718-735. DOI: 10.4236/ojg.2014.412052.

Simm, R., Bacon, M., 2014. Seismic amplitude: An interpreter's handbook. Cambridge University Press.